



UNIVERSITY OF LEEDS

This is a repository copy of *Population-specific modelling of between/within-subject flow variability in the carotid arteries of the elderly*.

White Rose Research Online URL for this paper:
<http://eprints.whiterose.ac.uk/151501/>

Version: Accepted Version

Article:

Lassila, T orcid.org/0000-0001-8947-1447, Sarrami-Foroushani, A, Hejazi, S et al. (1 more author) (2020) Population-specific modelling of between/within-subject flow variability in the carotid arteries of the elderly. *International Journal for Numerical Methods in Biomedical Engineering*, 36 (1). e3271. ISSN 2040-7939

<https://doi.org/10.1002/cnm.3271>

© 2019, John Wiley & Sons, Ltd. This is the peer reviewed version of the following article: Lassila, T, Sarrami-Foroushani, A, Hejazi, S, Frangi, AF. Population-specific modelling of between/within-subject flow variability in the carotid arteries of the elderly. *Int J Numer Meth Biomed Engng*. 2020; 36:e3271, which has been published in final form at <https://doi.org/10.1002/cnm.3271>. This article may be used for non-commercial purposes in accordance with Wiley Terms and Conditions for Use of Self-Archived Versions.

Reuse

Items deposited in White Rose Research Online are protected by copyright, with all rights reserved unless indicated otherwise. They may be downloaded and/or printed for private study, or other acts as permitted by national copyright laws. The publisher or other rights holders may allow further reproduction and re-use of the full text version. This is indicated by the licence information on the White Rose Research Online record for the item.

Takedown

If you consider content in White Rose Research Online to be in breach of UK law, please notify us by emailing eprints@whiterose.ac.uk including the URL of the record and the reason for the withdrawal request.



eprints@whiterose.ac.uk
<https://eprints.whiterose.ac.uk/>

RESEARCH ARTICLE – APPLICATION

Population-specific modelling of between/within-subject flow variability in the carotid arteries of the elderly

Toni Lassila¹ | Ali Sarrami-Foroushani¹ | SeyedMostafa Hejazi¹ | Alejandro F. Frangi¹

¹Centre for Computational Imaging & Simulation Technologies in Biomedicine (CISTIB), School of Computing, University of Leeds, United Kingdom

Correspondence

Toni Lassila, University of Leeds, EC Stoner Building, Leeds LS2 9JT, United Kingdom.
Email: t.lassila@leeds.ac.uk

Funding Information

This research was supported by the H2020 Programme project InSilc “*In-silico trials for drug-eluting BVS design, development and evaluation*” (H2020-SC1-2017-CNECT-2-777119); 7th Framework Programme project VPH-DARE@IT “*Virtual Physiological Human: Dementia Research Enabled by IT*” (FP7-ICT-2011-5.2-601055). The information contained herein reflects only the authors’ view and the European Commission is not responsible for any use that may be made of it.

Abstract

Computational fluid dynamics models are increasingly proposed for assisting the diagnosis and management of vascular diseases. Ideally, patient-specific flow measurements are used to impose flow boundary conditions. When patient-specific flow measurements are unavailable, mean values of flow measurements across small cohorts are used as normative values. In reality, both the between-subjects and within-subject flow variabilities are large. Consequently, neither one-shot flow measurements nor mean values across a cohort are truly indicative of the flow regime in a given person. We develop models for both the between-subjects and within-subject variability of internal carotid flow. A log-linear mixed effects model is combined with a Gaussian process to model the between-subjects flow variability, while a lumped parameter model of cerebral autoregulation is used to model the within-subject flow variability in response to heart rate and blood pressure changes. The model parameters are identified from carotid ultrasound measurements in a cohort of 103 elderly volunteers. We use the models to study intracranial aneurysm flow in 54 subjects under rest and exercise and conclude that OSI, a common wall shear-stress derived quantity in vascular CFD studies, may be too sensitive to flow fluctuations to be a reliable biomarker.

KEYWORDS:

computational fluid dynamics, cerebrovascular disease, patient-specific models, Gaussian process models, uncertainty quantification

1 | INTRODUCTION

Numerous computational fluid dynamics (CFD) models of human cardio- and cerebrovascular physiology are published every year, but few of them make any impact in clinical practice. This inconvenient truth has been blamed on the improper use of CFD solvers¹, insufficient validation of biomechanics models², and lack of understanding of the clinical decision-making process by the biomedical engineers building the models³. One additional explanation is that many “patient-specific” CFD models fail to consider the physiological variability of vascular flow, confounding interpretation of model results and producing overly confident predictions of flow quantities.

Patient-specific modelling of vascular flow requires an accurate description of the lumen plus the definition of boundary conditions. The latter is done by measuring patient-specific flow waveforms using either phase contrast magnetic resonance imaging (pcMRI) or ultrasound-based flow measurement techniques. When patient-specific flow measurements are not available,

cohort-averaged values of flow from the literature are often used. For example, the small-scale studies^{4,5,6} all used pcMRI to measure carotid flow in young healthy volunteers. Flow measurements in older adults were reported in⁷, and significant differences in the oscillatory shear index (OSI) were observed as a result of changing the flow waveforms from young adults to older adults⁸. Another study⁹ observed that flow rate variability has an effect on the predicted performance of flow-diverters in the treatment of intracranial aneurysms. Such results indicate that both the flow variability and the specific demographics of the target patient population should be taken into account in vascular CFD simulations¹⁰.

The uncertainty caused by not knowing the exact patient-specific flow can be quantified by running an ensemble of CFD simulations over a physiological range of flow variability. This allows the modeller to establish not only mean values but also variability bounds for the output quantities of interest. However, few large-scale studies have reported estimates of vascular flow variability in normal populations and many published vascular CFD studies still use only one or a handful of inlet flow waveforms to explore effects of flow variability, see e.g.^{11,12}. There is a risk that considering only small samples can lead to bias and underestimation of physiological flow variability. This, in turn, will lead to overconfidence in vascular CFD uncertainty quantification. More recently, statistical models of carotid flow variability have been proposed in the literature^{13,14} and used to perform uncertainty quantification of vascular CFD. While *between-subjects* flow variability is relatively straightforward to quantify by repeated measurements in a suitably selected cohort, a more informative measure would be *within-subject* flow variability i.e. multiple flow measurements in the same subject but over a series of physiological states (e.g. rest vs. exercise). The difficulty of performing *in-vivo* flow measurements outside the clinic then lead us to approach the problem by exploiting mathematical models of the cardiovascular system as surrogates.

The objectives of this study are: (i) identify key patient-specific vascular flow parameters, (ii) provide distributions of the flow parameters in a realistic elderly cohort, and (iii) develop data-driven and mechanistic models for both *between-subjects* and *within-subject* blood flow variability that explicitly incorporate demographic variables (age, sex, body size). Treatment of demographic variables is standard in biomedical studies, but relatively few attempts have been made so far to account for them in vascular flow models (see e.g.¹⁵). Our models will then provide: (i) cohort-specific boundary conditions to vascular CFD simulations in the case that patient-specific flow measurements are not available, and (ii) estimates of within-subject flow variability in cases where patient-specific flow measurements are available only as spot measurements.

Although the methods are general, to demonstrate the utility of the models we focus on internal carotid arterial (ICA) flow in the context of intracranial aneurysms. The flow in the left and right ICAs accounts for the majority of cerebral blood flow and is reported to have around 10-20% between-subjects variability in different studies^{4,16,17}. Mean flow varies less within-subject (<10%) due to the modulating effect of the cerebral autoregulation system, yet changes to the flow waveform can still be observed. In previous studies, it has been shown that changes in wall shear stress (WSS) induced by flow variability can significantly change the CFD-based predictions of intracranial aneurysm rupture risk^{14,12}. We consider within-subject flow variability induced by changes in systolic blood pressure (BP) and heart rate (HR) during physical exercise, and study the corresponding changes in WSS indicators, such as time-averaged WSS (TAWSS) or oscillatory shear index (OSI) in 54 subjects.

2 | MATERIALS AND METHODS

2.1 | Patient-specific vascular flow measurements

Patient-specific carotid flow data (*Lido cohort*) used in this study were part of an Alzheimer's disease study conducted at the Istituto di Ricovero e Cura a Carattere Scientifico San Camillo, Lido di Venezia, Italy, and previously reported in¹⁸. The cohort included 103 elderly people (age 73 ± 7 years), of whom 53 were diagnosed with mild cognitive impairment and the rest were healthy controls. Exclusion criteria included cerebrovascular disease as main aetiology, as well as the presence of any cardiovascular disease. The cohort could, therefore, be identified as elderly but healthy from the standpoint of vascular disease. The study was approved by the joint ethics committee of the Health Authority Venice 12 and the IRCCS San Camillo (Protocol number 2014.08) and all participants gave informed consent prior to participation.

To measure carotid flow, ultrasound imaging (Siemens Acuson X300PE, Siemens Healthineers, Erlangen, Germany) was performed. Both left and right internal carotid waveforms were digitised from the DICOM images using *im2graph* (Shai Vain-gast, www.im2graph.co.il). Time-averaged mean velocity signals were converted to flow rates by assuming fully developed flow and a circular cross-section, $q_{ICA}(t) = v_{TA,mean}(t)\pi r_{ICA}^2$, where the lumen radius was estimated by the cardiologist during the carotid ultrasound acquisition protocol. We also estimated the ICA velocity profiles in each subject by measuring the ratio

$v_{TA,max}/v_{TA,mean}$, and obtained a mean ratio of 1.65 ± 0.15 for the ICA-L and a mean ratio of 1.64 ± 0.19 for the ICA-R. Therefore we noted that in almost all cases the velocity profile was closer to parabolic than plug flow, and in several cases values of 1.8-1.9 were recorded, indicating a good fit of the parabolic profile assumption. The resulting flow rate signals were normalised to unit time and synchronised so that the maximum systolic upstroke point was matched between all the signals.

2.2 | Statistical modelling of between-subjects variability in ICA flow

We previously modelled between-subjects ICA flow variability in¹⁴, where data from 17 healthy young adults⁴ was used to train a Gaussian process model. In that work, the time-averaged mean flow rate was normalised for a given arterial diameter to achieve a time-averaged WSS of 1.5 Pa at the level of the carotid sinus. We extended this model to include also the between-subjects variability of the time-averaged flow.

The model was trained on log-transformed flow values to ensure that the predicted flow rates remained positive. The log-transformed ICA flow rates q_{ICA-L} and q_{ICA-R} were assumed to consist of two parts; the time-averaged mean flow, \bar{y}_{bs} , and the time-varying part (*waveform*), y_{bs}^* :

$$\begin{aligned}\log(q_{ICA-L}) &= \bar{y}_{bs,L} + y_{bs,L}^*, \\ \log(q_{ICA-R}) &= \bar{y}_{bs,R} + y_{bs,R}^*.\end{aligned}\quad (1)$$

For notational simplicity, we drop the indices L/R in what follows, keeping in mind that separate models were trained for both left and right carotid flow. The time-averaged part of the flow was modelled by a mixed-effects linear model:

$$\bar{y}_{bs} = \beta_0 + \beta_h x_{\text{height}} + \varepsilon = \beta_0 + \beta_h x_{\text{height}} + \sigma_{bs} \omega, \quad (2)$$

using height x_{height} as a fixed effect to account for the allometric dependence of cardiac output on body size¹⁹. The variance σ_{bs}^2 was estimated from the residuals of the linear model fit, and $\omega \in \mathcal{N}(0, 1)$ was the normal distribution. Separate effects were estimated for the male and female sub-cohorts.

The time-varying part of ICA flow, y_{bs}^* , was modelled as a Gaussian process:

$$y_{bs}^* = \mathcal{GP}(\sigma, t_i; \omega). \quad (3)$$

where $\{t_i\}_{i=1}^{\ell}$ were temporal landmarks that characterised the waveform shape. The flow rates at these landmark points were used to estimate the covariance matrix:

$$\Sigma = \begin{bmatrix} \Sigma^{LL} & \Sigma^{LR} \\ \Sigma^{RL} & \Sigma^{RR} \end{bmatrix}, \quad (4)$$

where $\Sigma_{i,j}^{LR} := \text{cov} \left[y_{bs,L}^*(t_j), y_{bs,R}^*(t_i) \right]$ is the covariance between the log-transformed left and right carotid waveforms $y_{bs,L}^*$, $y_{bs,R}^*$ (and similarly for the other sub-matrices). Again, the covariances were estimated separately for each sex. The between-subjects variability model fitting process is graphically represented in Fig. 1.

2.3 | Statistical modelling of within-subject variability in ICA flow

Within-subject variability in ICA flow arises mainly due the changes in cardiac output, quantified here by heart rate (HR) and systolic blood pressure (SBP). These changes are modulated by the cerebral autoregulation system (CARS) that includes myogenic (pressure-driven), shear-induced (flow-driven), and metabolic (energy-driven) regulation mechanisms. To model within-subject variability of carotid flow, we considered a range of arterial BP waveforms with different values of HR and SBP and used a mathematical model of the CARS to generate the corresponding flow rate waveforms.

The CARS model of Mader *et al.*²⁰ is a two-element feedback controller, for which orthostatic stress tests were previously used to identify model parameters in both middle-aged and elderly volunteers:

$$\left\{ \begin{aligned} \frac{dv_1}{dt} &= -(a + b + c)v_1(t) + (c - d(t))v_2(t) + (a + b)p(t) \\ \frac{dv_2}{dt} &= -bv_1(t) - d(t)v_2(t) + bp(t) \\ d(t) &= \frac{bc f_{aut}(t)}{Mc p(t) - (a + c)f_{aut}(t)} \\ f_{aut}(t) &= 2.03 \cdot 10^{-6} p(t)^3 - 6.02 \cdot 10^{-4} p(t)^2 + 5.94 \cdot 10^{-2} p(t) - 1.95 \end{aligned} \right., \quad (5)$$

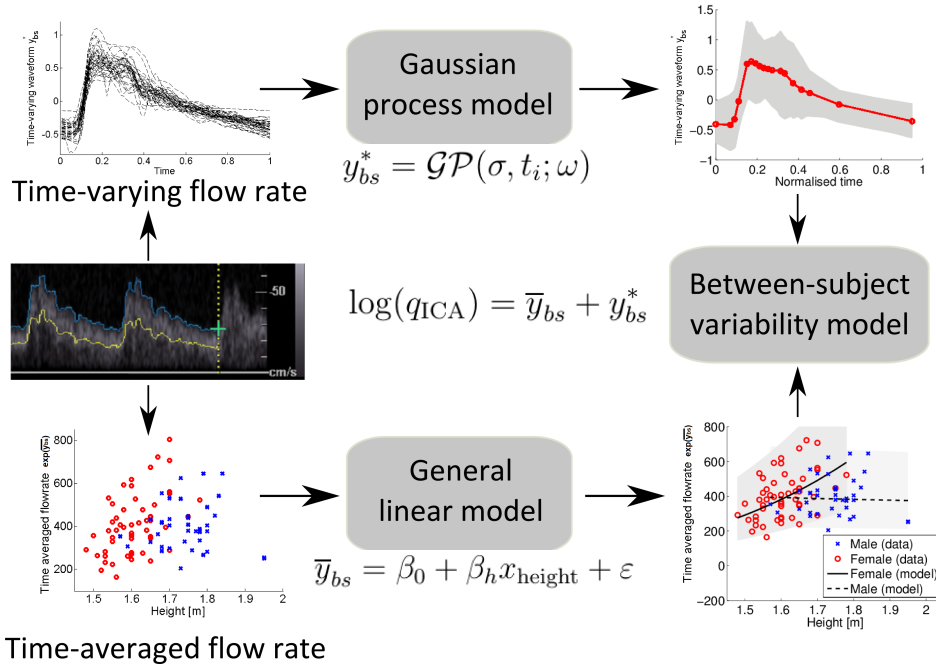


FIGURE 1 Training of the between-subjects flow variability -model (1).

where a , b , and c are nonnegative parameters of the two-element viscoelastic Voigt -model for predicting responses to fluctuating pressure, and $d(p)$ includes the pressure-dependent resistance. The relation $f_{aut}(p)$ represents the cerebral autoregulation curve, and M is the amplification factor of the CBF fluctuation. The model parameters were calibrated for both middle-aged (a_m, b_m, c_m, M_m) and elderly subjects (a_e, b_e, c_e, M_e) in²⁰ using orthostatic tests²⁰. We modelled the dependency on age x_{age} by blending piecewise linearly between the two sets of parameters:

$$\begin{aligned} a &= a_m \lambda + (1 - \lambda) a_e, & b &= b_m \lambda + (1 - \lambda) b_e, \\ c &= c_m \lambda + (1 - \lambda) c_e, & M &= M_m \lambda + (1 - \lambda) M_e \end{aligned} \quad (6)$$

where

$$\lambda = \begin{cases} 1, & \text{if } x_{age} < 35 \\ \frac{75 - x_{age}}{40}, & \text{if } 35 \leq x_{age} \leq 75 \\ 0, & \text{if } x_{age} > 75 \end{cases} \quad (7)$$

Finally, the flow velocity in the middle cerebral artery (MCA) was obtained as:

$$v_{MCA}(t) = M(p(t) - v_1(t)) + \bar{v}, \quad (8)$$

where \bar{v} corresponds to the time-averaged flow velocity. To translate MCA flow velocities to ICA flow rates, we assumed a linear relationship between ICA and MCA flows:

$$q_{ICA} = \gamma A_{ICA} v_{MCA}, \quad (9)$$

where A_{ICA} was the cross-sectional area of the ICA, and the VMCA/VICA index was $\gamma = 1.67 + 0.005 \times x_{age}$ for women and $\gamma = 2.00$ for men, as proposed in²¹.

To drive the CARS model, the BP waveform $p(t)$ needed to be specified. For a given reference HR, we assumed there exists a reference BP signal $p_{ref}(t)$ with SBP $p_{s,ref}$ and DBP $p_{d,ref}$. The effect of HR and SBP variability on BP was then obtained by rescaling the reference BP waveform:

$$p(t; \tau, p_s, p_d) = \frac{p_{ref}\left(\frac{\tau_{ref}}{\tau} t\right) - p_{d,ref}}{p_{s,ref} - p_{d,ref}} (p_s - p_d) + p_d. \quad (10)$$

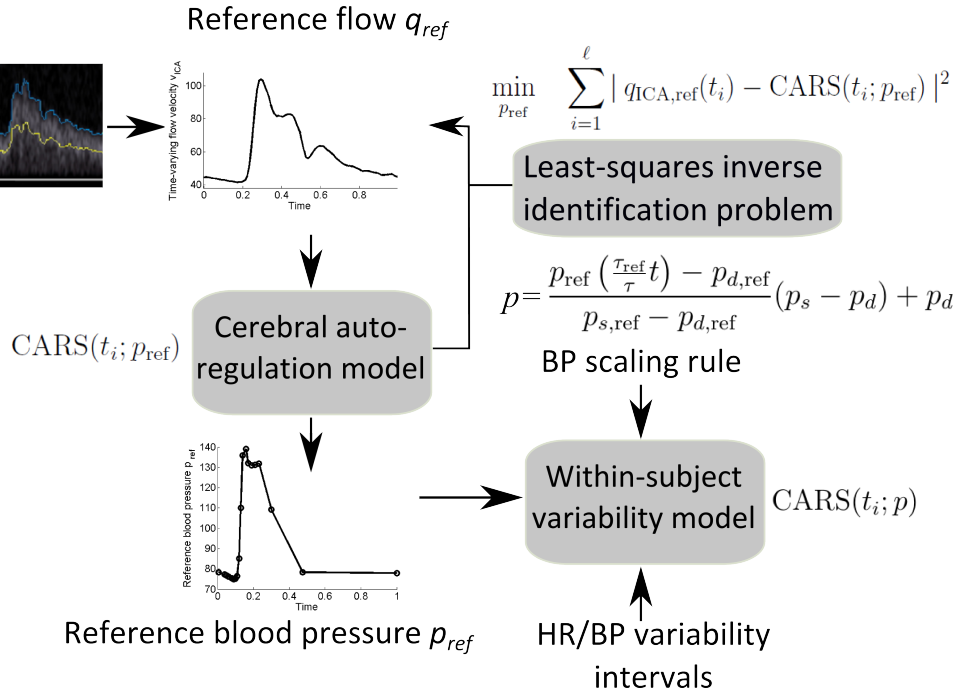


FIGURE 2 Training of the within-subject flow variability -model (5)–(8).

where $\tau = 60/\text{HR}$ is the cardiac interval. Since BP waveforms were not available in this cohort, we used an inverse procedure to recover the reference BP from the ultrasound flow measurement by solving the least squares problem:

$$\min_{p_{\text{ref}}} \sum_{i=1}^{\ell} |q_{\text{ICA,ref}}(t_i) - \text{CARS}(t_i; p_{\text{ref}})|^2, \quad (11)$$

where $\text{CARS}(t_i; p_{\text{ref}})$ is the output of the CARS model at time t_i when driving the model with the reference pressure $p_{\text{ref}}(t)$, and $q_{\text{ICA,ref}}$ is the reference ICA flow waveform. The within-subject variability model fitting process is graphically represented in Fig. 2.

2.4 | Study on the effect of exercise on aneurysm flow

To demonstrate the utility of intra-subject flow variability models, we studied the specific case of flow prediction in intracranial aneurysms (IAs). Aneurysms are outcomes of vascular disease characterised by the incremental growth of a saccular extrusion of the blood vessel that, over time, may rupture, leading to permanent morbidity or death. The mechanobiological growth and rupture process of IAs has been linked to changes in wall shear stress (WSS) patterns. A number of CFD studies^{22,14,12} have looked at the effect of cerebral blood flow (CBF) fluctuations in WSS patterns, but none to our knowledge have considered the effect of the CARS. Quantities of interest include time-averaged WSS (TAWSS), oscillatory shear index (OSI), and transverse WSS (TransWSS):

$$\begin{aligned} \text{TAWSS}(x) &= \frac{1}{T_{\text{period}}} \int_{T_0}^{T_0+T_{\text{period}}} |\boldsymbol{\tau}_w(x, t)| dt; \\ \text{OSI}(x) &= \frac{1}{2} \left(1 - \frac{\left| \int_{T_0}^{T_0+T_{\text{period}}} \boldsymbol{\tau}_w(x, t) dt \right|}{\int_{T_0}^{T_0+T_{\text{period}}} |\boldsymbol{\tau}_w(x, t)| dt} \right); \\ \text{TransWSS}(x) &= \frac{1}{T_{\text{period}}} \int_{T_0}^{T_0+T_{\text{period}}} |\boldsymbol{\tau}_w(x, t) \cdot (\hat{p} \times \hat{n})| dt, \end{aligned} \quad (12)$$

where \hat{n} is the surface normal, and the unit vector \hat{p} in the direction of the time-averaged WSS vector can be calculated as:

$$\hat{p}(x) = \frac{\int_{T_0}^{T_0+T_{\text{period}}} \boldsymbol{\tau}_w(x, t) dt}{\left| \int_{T_0}^{T_0+T_{\text{period}}} \boldsymbol{\tau}_w(x, t) dt \right|}. \quad (13)$$

To enable comparison of TransWSS across cases, we calculated the relative TransWSS (rTransWSS) as the TransWSS normalised by the TAWSS at each surface point¹⁴. All point-wise quantities were averaged over the aneurysmal sac and used for population-specific analyses. Previous studies indicate that endothelial regions at-risk of rupture can be characterised as having low TAWSS but highly fluctuating WSS (both high OSI and high TransWSS)²³. As a sudden rise in blood pressure may trigger the rupture of an aneurysm^{24,25}, we investigated whether changes in CBF experienced in hypertensive conditions play a role in altering the WSS patterns.

To generate a virtual cohort of IAs to test the differences in WSS between rest vs. exercise, patient-specific vascular surface models ($N = 54$) were segmented from previously acquired 3-D rotational angiography images in the @neurIST project²⁶. Vascular models were discretised using unstructured volumetric meshes in ANSYS ICEM v16.2 (Ansys Inc., Canonsburg, PA, USA). Tetrahedral elements with maximum edge size of 0.2 mm were used and three layers of prismatic elements with an edge size of 0.1 mm were used to create boundary layers. Blood flow in the IA was modelled using the unsteady Navier-Stokes equations. Blood was assumed to be an incompressible Newtonian fluid with a density of 1066 kg/m³ and viscosity of 0.0035 Pa·s. The vessel walls were assumed to be rigid. To ensure fully developed flow, the computational domain was extended at the inlet boundary by an entrance length proportional to the inlet boundary maximum Reynolds number. The Navier-Stokes equations were solved in ANSYS CFX v16.2 (Ansys Inc., Canonsburg, PA, USA). The cardiac cycle was discretised in time into 200 equal steps. Element and time-step sizes were set according to the neurIST processing toolchain, where mesh convergence tests were performed on WSS, pressure, and flow velocity at several points in the computational domain as described by²⁶. Boundary layer meshes were used to improve WSS accuracy.

No patient-specific flow measurements were available in the @neurIST cohort. Instead, the mean waveform (different for men/women) from the Lido cohort was used as the baseline flow waveform. The baseline waveform was used as inlet boundary condition (velocity) to the CFD models of aneurysm flow at rest. To enable population-wide comparisons, Poiseuille's law was used to scale the mean waveform such that the time-averaged WSS was 1.5 Pa at the inlet for each patient (elimination of mean effect). A parabolic inflow profile was used in all cases, but given a sufficiently long extension at the inlet of the domain the CFD results were independent of the inlet velocity profile. We modeled differences in the inlet flow waveform between rest and exercise by increasing the HR from 66 bpm (at rest) to an elevated level of 145 bpm (during exercise), i.e., an increase by a factor of 2.2²⁷. These values were used as parameters in the within-subject flow variability model of Sect. 2.3. The baseline pressure waveform was determined for each case by solving problem (11). After solving the inverse problem, the systolic BP was correspondingly increased by a factor of 1.3²⁷ in formula (10) to simulate effects of exercise and used to drive the CARS model and obtain the ICA waveform. The ICA waveforms were then used as inlet boundary condition to the CFD models of aneurysm flow during exercise. Zero-pressure boundary conditions were imposed at all outlets. **While this boundary condition does not necessarily lead to a physiological flow split between the outlet branches, it is used in many CFD studies due to the difficulty of determining patient-specific values of the outlet resistances²⁸. The other commonly used way to compute flow splits between arterial branches, Murray's law, has been found to be violated in the circle of Willis²⁹. The zero-pressure condition was chosen here as a compromise to obtain CFD results that were comparable between different cases without introducing additional parameters that would require tuning on a case-by-case -basis.**

3 | RESULTS

3.1 | Cohort statistics for flow variables

Summary statistics of the Lido cohort are presented in Table 1. Differences between the sexes were observed in body size, left ventricular volume/mass, and carotid artery diameters. Carotid flow velocity waveforms were extracted from both ICA-L and ICA-R for $N = 92$ study participants. For $N = 11$ participants carotid examination failed in either one or both sides and no signal could be analysed. The log-transformed carotid flow rates after subtracting the time-averaged mean flow are presented in Fig. 3, for men and women separately. The coefficient of variation in the time-averaged flow was 34% for ICA-L and 39% for ICA-R, indicating large between-subjects variability. Qualitative evaluation of the cohort mean waveforms indicated that a

TABLE 1 Carotid flow measurements in an elderly cohort presented by population mean (std dev). Differences between the sexes are exhibited in body size and mass, left ventricle size and mass, and carotid artery diameters. Univariate p -values were computed by one-way ANOVA. Statistical significance with $p < 0.05$ is denoted by * and with $p < 0.001$ is denoted by **.

Demographics	Male	Female	p -value
N	41	62	
Age [y]	73 (9)	74 (6)	0.691
Height [cm]	174 (7)	161 (7)	< 0.001**
Weight [kg]	80 (13)	65 (12)	< 0.001**
Body-mass index	26.5 (3.3)	25.0 (3.8)	0.041*
Carotid arteries			
Intima-media thickness CCA-L [mm]	0.87 (0.20)	0.83 (0.18)	0.302
Intima-media thickness CCA-R [mm]	0.88 (0.21)	0.84 (0.17)	0.329
Mean time-averaged velocity ICA-L [cm/s]	17.5 (3.9)	19.6 (5.3)	0.031*
Mean time-averaged velocity ICA-R [cm/s]	18.2 (4.8)	18.9 (5.1)	0.491
Mean time-averaged velocity CCA-L [cm/s]	21.5 (6.4)	20.8 (4.9)	0.558
Mean time-averaged velocity CCA-R [cm/s]	21.5 (6.1)	19.6 (5.2)	0.101
Mean time-averaged velocity ECA-L [cm/s]	16.3 (5.2)	14.9 (4.2)	0.144
Mean time-averaged velocity ECA-R [cm/s]	16.6 (5.7)	16.3 (5.4)	0.763
Diameter ICA-L [mm]	7.1 (1.0)	6.6 (0.9)	0.009*
Diameter ICA-R [mm]	7.0 (1.0)	6.5 (0.9)	0.009*
Diameter CCA-L [mm]	7.0 (0.7)	6.6 (0.6)	0.001*
Diameter CCA-R [mm]	7.1 (0.8)	6.7 (0.6)	0.002*
Diameter ECA-L [mm]	5.0 (0.5)	4.6 (0.6)	0.002*
Diameter ECA-R [mm]	4.9 (0.5)	4.6 (0.6)	0.010*
Mean time-averaged flow rate ICA-L [ml/min]	429 (135)	411 (149)	0.526
Mean time-averaged flow rate ICA-R [ml/min]	437 (169)	382 (148)	0.087

more prominent dicrotic notch was present in males than in females. It is clear that using a single “normative” waveform to characterise this cohort will not produce credible CFD simulations.

3.2 | Between-subjects flow variability -model

The mean flow rate of each carotid waveform was computed and the values used to fit the log-linear mixed effects model for \bar{y}_{bs} . The model fit is represented graphically in Fig. 4. The estimated effects for men and women in the ICA-L and ICA-R are given in Table 2. The fixed effect for height was statistically significant in women ($\beta_{h,L} = 4.165$, $p < 0.001$ and $\beta_{h,R} = 2.944$, $p = 0.01$), but not in men ($\beta_{h,L} = -0.224$, $p = 0.0825$ and $\beta_{h,R} = 0.200$, $p = 0.886$). In previous studies, cardiac stroke volume was associated with height following an allometric scaling law with power $\beta_h = 2.04$ (in adults)¹⁹.

After subtracting the time-averaged component from the log-transformed ultrasound signals, $\ell = 18$ landmark points were selected manually to avoid ill-conditioning of the sample covariance matrix (4) when the upstroke of the waveform is sampled at points that are clustered very closely together. Once the Gaussian process models were trained for both men and women, they were used to generate a virtual waveform sample of 103 cases, where the sample size was chosen to match that of the original data used for model training in order to obtain comparable sample variances. The statistics of this virtual cohort were compared to the original cohort by applying the Kolmogorov-Smirnov -test (Table 3). The distribution of flow parameters in the resulting virtual cohort was statistically indistinguishable from the original cohort, indicating successful model training.

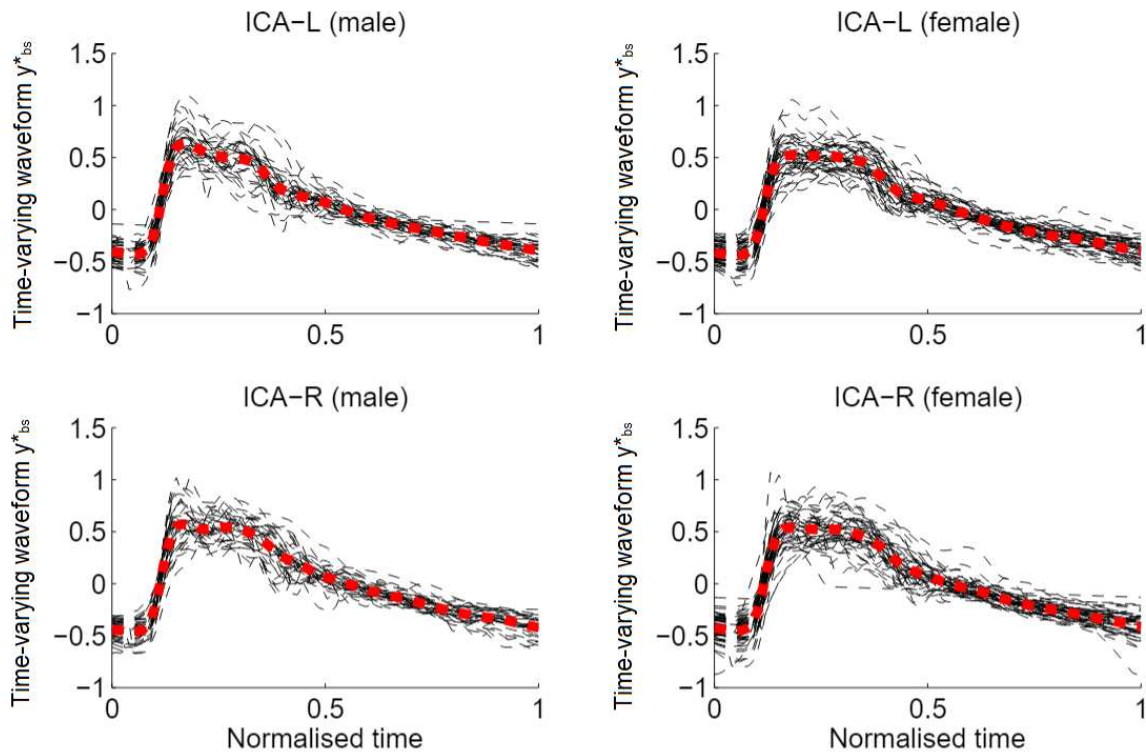


FIGURE 3 Log-transformed ICA flow waveforms in the study cohort in males (left column, $N = 38$) and females (right column, $N = 52$) after subtracting the temporal mean from each signal. Cohort mean waveform overlaid in red. Flow rate measured in logarithm of ml/min.

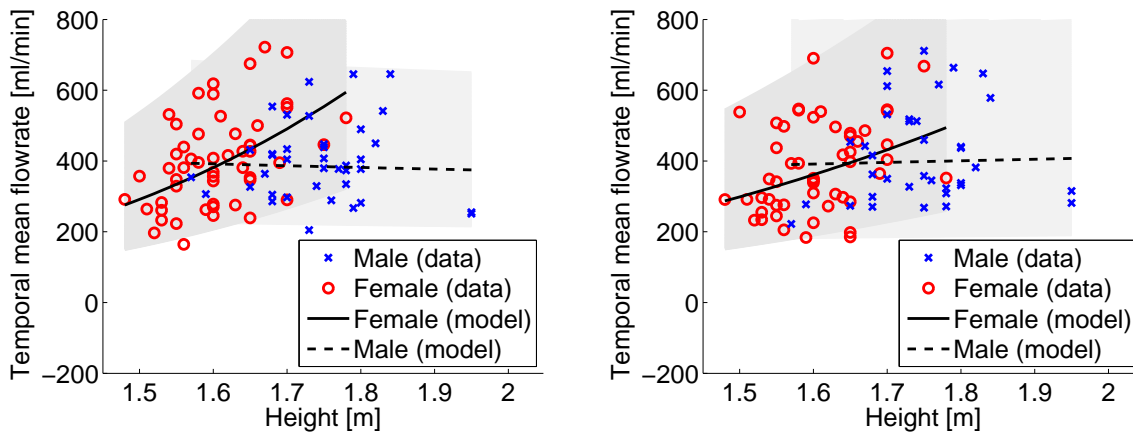


FIGURE 4 Mixed-effects log-linear model for temporal mean flow in the ICA-L (left) and ICA-R (right). Separate models are trained for males and females. Shaded area represents the 95% confidence intervals.

3.3 | Study on the effect of exercise on aneurysm flow

Flow variability in the host artery (either the internal carotid, middle cerebral, or posterior communicating artery) during rest and exercise was measured with two different indicators: mean flow (FLOW) and pulsatility index (PI). The variabilities of these indicators as well as the WSS-related quantities measured in the aneurysm are reported in Table 4. Due to the effects of the CARS, FLOW only fluctuated moderately ($< 10\%$) even when the HR was increased considerably. Meanwhile, the PI increased

TABLE 2 Parameters of the mixed effects model for \bar{y}_{bs} , their 95%-confidence intervals, and p -values. Height had a statistically significant effect in women but not in men. Statistical significance with $p < 0.05$ is denoted by * and with $p < 0.001$ is denoted by **.

Model parameter, men	Value	Confidence interval	p -value
Time-averaged flow rate ICA-L, β_0	6.077	(4.952 – 7.201)	< 0.001**
Time-averaged flow rate ICA-L, β_h	-0.224	(-2.242 – 1.793)	0.825
Time-averaged flow rate ICA-R, β_0	5.875	(4.330 – 7.421)	< 0.001**
Time-averaged flow rate ICA-R, β_h	0.200	(-2.573 – 2.973)	0.886
Stdev of residuals ICA-L, σ_L	0.275		
Stdev of residuals ICA-R, σ_R	0.378		

Model parameter, women	Value	Confidence interval	p -value
Time-averaged flow rate ICA-L, β_0	3.986	(2.982 – 4.990)	< 0.001**
Time-averaged flow rate ICA-L, β_h	4.165	(2.052 – 6.277)	< 0.001**
Time-averaged flow rate ICA-R, β_0	4.506	(3.452 – 5.559)	< 0.001**
Time-averaged flow rate ICA-R, β_h	2.944	(0.727 – 5.160)	0.010*
Stdev of residuals ICA-L, σ_L	0.305		
Stdev of residuals ICA-R, σ_R	0.320		

TABLE 3 Population mean (std dev) of flow parameters measured by ultrasound versus simulated by the between-subjects variability model (1). Distributions compared using the Kolmogorov-Smirnov -test, significant difference with $p < 0.05$ is denoted by * and with $p < 0.001$ is denoted by **.

Flow parameter, women	Ultrasound	Model (1)	p -value
Time-averaged flow rate ICA-L [ml/min]	433 (146)	438 (159)	0.953
Time-averaged flow rate ICA-R [ml/min]	409 (135)	414 (149)	0.964
Pulsatility index ICA-L	1.14 (0.24)	1.16 (0.24)	0.475
Pulsatility index ICA-R	1.20 (0.27)	1.22 (0.24)	0.146
Resistivity index ICA-L	0.65 (0.07)	0.65 (0.07)	0.483
Resistivity index ICA-R	0.66 (0.07)	0.67 (0.07)	0.277

Flow parameter, men	Ultrasound	Model (1)	p -value
Time-averaged flow rate ICA-L [ml/min]	424 (118)	425 (119)	0.992
Time-averaged flow rate ICA-R [ml/min]	454 (177)	455 (175)	0.906
Pulsatility index ICA-L	1.29 (0.30)	1.31 (0.27)	0.315
Pulsatility index ICA-R	1.29 (0.27)	1.30 (0.25)	0.884
A Resistivity index ICA-L	0.68 (0.07)	0.68 (0.06)	0.850
Resistivity index ICA-R	0.68 (0.07)	0.69 (0.06)	0.938

by over 100% in certain cases. In practice, all WSS-related indicators (TAWSS, OSI, rTransWSS) experienced on average an increase when moving from rest to exercise (Table 4). By far the largest increase was observed in OSI, which more than doubled on average during exercise. rTransWSS was considerably less sensitive to flow fluctuations, being only somewhat more sensitive than TAWSS. In our previous study¹⁴ TransWSS was similarly found to be a smoother measure of WSS fluctuations.

Changes in the absolute values of WSS and OSI might have relatively little physiological meaning unless critical thresholds are met for upregulating atheroprotective (for high TAWSS) or inflammatory pathways (low TAWSS and high OSI) in the endothelium. Therefore, we also studied areas of low TAWSS (defined as TAWSS < 0.4 Pa) and high OSI (defined as OSI > 0.4) relative to the total area of the aneurysmal sac. Their changes are also reported in Table 4. It was observed that relative

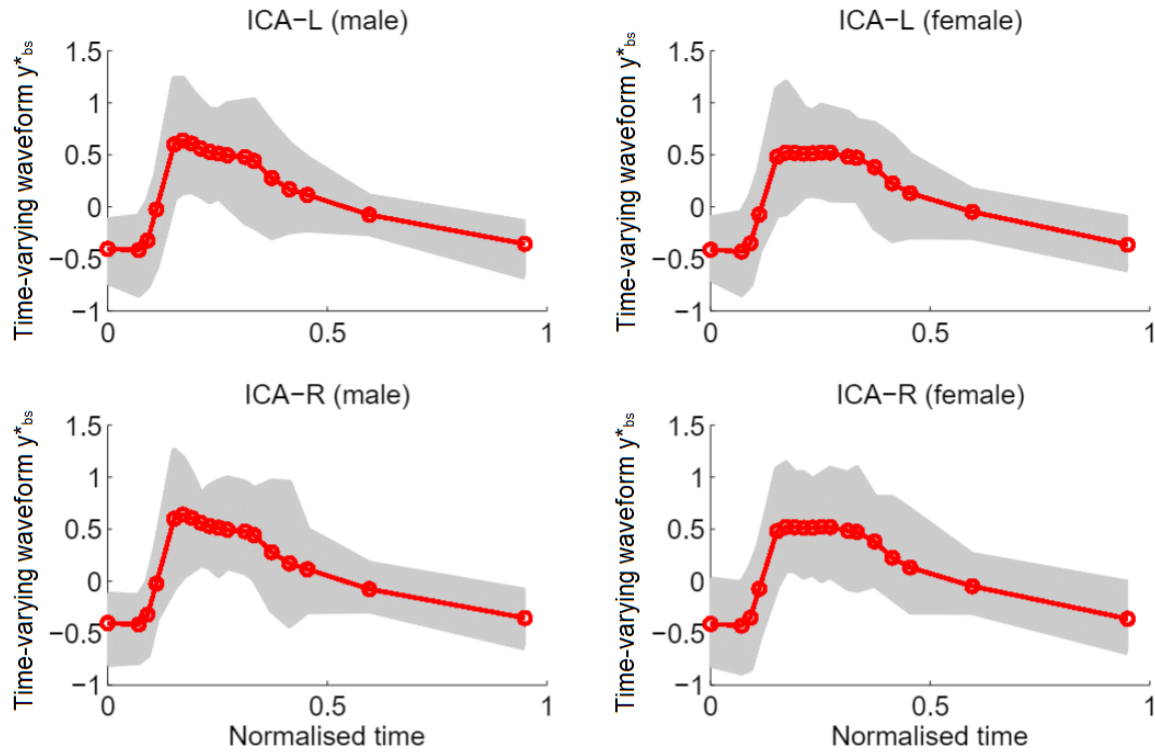


FIGURE 5 Gaussian process model for ICA flow fluctuation term in males (left column, $N = 38$) and females (right column, $N = 52$). Process mean waveform and landmarks overlaid in bold, variability bounds in gray.

TABLE 4 Population mean (std dev) of within-subject variability of flow- and WSS-related quantities in $N = 54$ intracranial aneurysms.

Indicator	Rest	Exercise	Relative difference
FLOW [ml/min]	240 (99)	245 (109)	2.00% (2.22%)
PI	1.18 (0.00)	2.13 (0.16)	80.3% (13.5%)
TAWSS	4.78 (4.17)	5.78 (4.93)	27.2% (19.6%)
OSI	0.027 (0.023)	0.053 (0.035)	124.0% (84.1%)
rTransWSS	0.168 (0.069)	0.240 (0.084)	48.1% (29.3%)
rArea Low TAWSS [%]	12.87 (22.07)	7.42 (15.04)	-58.6% (27.8%)
rArea High OSI [%]	2.30 (2.60)	5.09 (5.37)	165% (143%)

area of low TAWSS decreased on average, while the relative area of high OSI increased. To understand better the interplay of TAWSS and OSI, in Fig. 6 we present the case of a 41-year-old woman with a posterior communicating artery aneurysm. In this case, a large increase in host vessel pulsatility ($\Delta PI = 102\%$) lead to a corresponding large increase in TAWSS ($\Delta TAWSS = 39\%$) and OSI ($\Delta OSI = 129\%$). It should be noted that OSI tends to be a spatially concentrated measure of flow variability, so that even a large increase in OSI only affects a small part of the aneurysmal wall. At the same time, while TAWSS increased in most regions it remained low in the region where OSI was simultaneously elevated. Thus the actual change in rupture risk should be evaluated based on a combined informations about TAWSS and WSS pulsatility indicators, including analysis of the spatial patterns of WSS.

Linear correlations between changes in flow vs. changes in WSS are reported in Table 5. It was found that, on average, TAWSS increases were associated increases in both FLOW and PI, while the correlations between flow and OSI/rTransWSS changes were not statistically significant.

TABLE 5 Correlation coefficients between flow variability in the host artery (ICA) and WSS variability in $N = 54$ intracranial aneurysm.

Comparison	Pearson's ρ	p -value
Δ FLOW vs. Δ TAWSS	0.277	0.043*
Δ FLOW vs. Δ OSI	-0.132	0.340
Δ FLOW vs. Δ rTransWSS	-0.100	0.473
Δ FLOW vs. Δ rAreaLowTAWSS	-0.276	0.069
Δ FLOW vs. Δ rAreaHighOSI	-0.064	0.649
Δ PI vs. Δ TAWSS	0.430	0.001*
Δ PI vs. Δ OSI	-0.200	0.148
Δ PI vs. Δ rTransWSS	-0.225	0.102
Δ PI vs. Δ rAreaLowTAWSS	-0.183	0.237
Δ PI vs. Δ rAreaHighOSI	-0.101	0.469

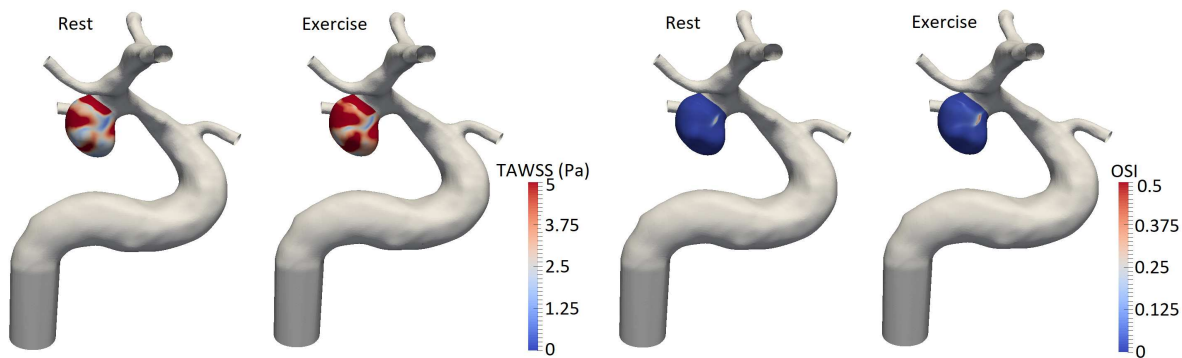


FIGURE 6 Example of flow in a posterior communicating artery aneurysm of a 41-year old female where a large increase in host vessel pulsatility (Δ PI = 102%) leads to corresponding large increases in TAWSS (Δ TAWSS = 39%) and OSI (Δ OSI = 129%).

4 | DISCUSSION

Computational fluid dynamics modelling is a promising tool for virtual treatment planning in cardio- and cerebrovascular disease, but requires patient-specific boundary conditions to achieve results that are relevant to the specific patient's physiology. If normative flow boundary conditions are used instead, derived quantities of flow, such as WSS, may incur large errors and uncertainties. In the context of intracranial aneurysm flow modelling, previous meta-analysis¹⁰ showed that the use of patient-unspecific boundary conditions leads to a moderate-sized effect (Hedges' $g = 0.30$) when evaluating WSS patterns on the aneurysmal endothelium. This uncertainty can be multiplied by the presence of within-subject flow variability. However, in clinical practice only a single flow measurement is usually performed and no estimate of systemic variability is available to guide the modeller as to the variability in the flow measurements.

We developed a within-subject flow variability model that mimics the response of the cerebral autoregulation system to cardiac output variability. This model can be used to extend a single baseline carotid flow measurement to a range of CBF experienced during the person's daily activities. As a concrete example, we performed CFD simulations in 54 intracranial aneurysms where the intra-subject flow variability model was used to generate waveforms at rest and during physical activity. Our results showed that physiological changes in CBF during increased physical activity may induce fluctuations an order of magnitude higher in certain WSS-related quantities, such as OSI (a 2% mean increase in flow lead to a 124% mean increase in OSI in our virtual cohort). This indicates that OSI may be too sensitive to flow uncertainty to be reliably used for rupture-risk evaluation. A partial recipe to this problem is to use alternative WSS indicators that are robust to flow fluctuations. We showed that TransWSS was less sensitive to flow fluctuations than OSI and, given a choice between the two, TransWSS should in our view be preferred over OSI when predicting IA rupture risk.

Sometimes it is simply not feasible to perform patient-specific flow measures in all the relevant locations of the vascular tree. In such cases, using normative flow values may be a necessity, but the uncertainty created by missing patient-specific measurements should be properly quantified. Recent studies^{13,14,12} have looked at between-subjects cerebral flow variability by combining data and mathematical modelling to quantify the CBF uncertainty. We developed a data-driven between-subjects flow variability model for ICA flow in elderly dementia patients and age-matched controls. The model was an extension of our previously developed model¹⁴ but also included a fixed-effects model using height and sex as predictors for time-averaged mean flow. By training separate models for men and women, sex-specific differences of the cerebrovascular physiology can be studied.

Besides patient-specific models, a separate paradigm that has arisen lately is what we call “*population-specific modelling*”. Instead of modelling the flow in a single patient, we generate a virtual population of waveforms that matches the statistical distribution of flow observed in a real patient cohort. The utility of virtual populations lies in the idea of *virtual in silico trials*, where medical treatments and devices can be tested using computer simulation. This can help reduce the size of actual clinical trials. By combining vascular surface models from a real cohort of patients and a between-subjects flow variability model, we can generate *virtual chimera patients* that extend the cohort beyond that which would be available with purely patient-specific data collection. It has been acknowledged that virtual patient models must incorporate both patient variability and the model uncertainty to augment clinical trials³⁰. Our model provides one of the necessary ingredients to successful virtual trials of cerebrovascular interventions.

Limitations: Our data-driven model for between-subjects CBF variability was based on ~ 100 participants from an ethnically homogeneous cohort (retirees from an island community in the Mediterranean). As data from larger, cross-sectional population studies become available (e.g. the UK Biobank project³¹), the models can be retrained for increased coverage and to achieve actual population-specific, not just cohort-specific models. The within-subject CBF variability was controlled by a simple autoregulation model that only considers short-term effects through changes in heart rate (HR) and systolic blood pressure. Long-term response to chronic disruptions in CBF, such as cardiac disease, should be modelled using a more advanced autoregulation model. Short-term effects such as beat-to-beat heart rate variability (HRV) effects were also not included in this study. Since HRV depends on many factors, such as current heart rate (inverse relation between HR and HRV), stress, nutrition, vascular fitness etc., the currently available data did not allow for modelling these subtle effects. However, if our assumption is correct that the CARS model can reasonably predict the response of the CARS to changes in HR, then provided that further stochastic models for HRV can be developed, they could consequently be used to feed the CARS and include also the effect of HRV. In order to validate our within-subject CBF variability model, it would be necessary to perform patient-specific measurements of CBF during rest and exercise. In the future, transcranial Doppler (TCD) may provide a non-invasive way to perform CBF measurements, and has been shown to be applicable also to studying CBF under conditions of light exercise, as was done by Fisher *et al.*³².

A MATLAB implementation of the between-subjects variability model is available at: <https://figshare.com/s/74cee398a83618e5ea08>.

ACKNOWLEDGEMENTS

We acknowledge A. Venneri, M. Mitolo, and F. Meneghello from IRCCS San Camillo as well as the @neurIST project for the clinical data collection, and M. Lange for assistance in the data processing. T. Lassila, A. Sarrami-Foroushani, and A.F. Frangi were funded by the H2020 Programme project InSilc “*In-silico trials for drug-eluting BVS design, development and evaluation*” (H2020-SC1-2017-CNECT-2-777119). T. Lassila and A.F. Frangi were funded by the 7th Framework Programme project VPH-DARE@IT “*Virtual Physiological Human: Dementia Research Enabled by IT*” (FP7-ICT-2011-5.2-601055). The information contained herein reflects only the authors’ view and the European Commission is not responsible for any use that may be made of it.

CONFLICTS

None declared.

References

1. Valen-Sendstad K, Steinman DA. Mind the gap: impact of computational fluid dynamics solution strategy on prediction of intracranial aneurysm hemodynamics and rupture status indicators. *Am J Neuroradiol.* 2014; 35(3): 536–543.
2. Anderson AE, Ellis BJ, Weiss JA. Verification, validation and sensitivity studies in computational biomechanics. *Comput. Methods Biomech. Biomed. Eng.* 2007; 10(3): 171–184.
3. Huberts W, Heinen SGH, Zonnebeld N, et al. What is needed to make cardiovascular models suitable for clinical decision support? A viewpoint paper. *J. Comput. Sci.* 2018; 24: 68–84.
4. Ford MD, Alperin N, Lee SH, Holdsworth DW, Steinman DA. Characterization of volumetric flow rate waveforms in the normal internal carotid and vertebral arteries. *Physiol. Measur.* 2005; 26(4): 477.
5. Holdsworth DW, Norley CJD, Frayne R, Steinman DA, Rutt BK. Characterization of common carotid artery blood-flow waveforms in normal human subjects. *Physiol. Measur.* 1999; 20(3): 219.
6. Marshall I, Papathanasopoulou P, Wartolowska K. Carotid flow rates and flow division at the bifurcation in healthy volunteers. *Physiol. Measur.* 2004; 25(3): 691.
7. Hoi Y, Wasserman BA, Xie YJ, et al. Characterization of volumetric flow rate waveforms at the carotid bifurcations of older adults. *Physiol. Measur.* 2010; 31(3): 291.
8. Xu L, Liang F, Zhao B, Wan J, Liu H. Influence of aging-induced flow waveform variation on hemodynamics in aneurysms present at the internal carotid artery: A computational model-based study. *Comput. Biol Med.* 2018; 101: 51–60.
9. Morales HG, Bonnefous O, Geers AJ, et al. Does arterial flow rate affect the assessment of flow-diverter stent performance?. *Am. J. Neuroradiol.* 2016; 37(12): 2293–2298.
10. Sarrami-Foroushani A, Lassila T, Frangi AF. Virtual endovascular treatment of intracranial aneurysms: models and uncertainty. *Wiley Interdiscip. Rev. Syst. Biol. Med.* 2017; 9(4).
11. Shimogonya Y, Kumamaru H, Itoh K. Sensitivity of the gradient oscillatory number to flow input waveform shapes. *J. Biomech.* 2012; 45(6): 985–989.
12. Xiang J, Siddiqui AH, Meng H. The effect of inlet waveforms on computational hemodynamics of patient-specific intracranial aneurysms. *J. Biomech.* 2014; 47(16): 3882–3890.
13. Durka MJ, Wong IH, Kallmes DF, et al. A data-driven approach for addressing the lack of flow waveform data in studies of cerebral arterial flow in older adults. *Physiol. Measur.* 2018; 39(1): 015006.
14. Sarrami-Foroushani A, Lassila T, Gooya A, Geers AJ, Frangi AF. Uncertainty quantification of wall shear stress in intracranial aneurysms using a data-driven statistical model of systemic blood flow variability. *J. Biomech.* 2016; 49(16): 3815–3823.
15. Biehler J, Kehl S, Gee MW, et al. Probabilistic noninvasive prediction of wall properties of abdominal aortic aneurysms using Bayesian regression. *Biomech. Model. Mechanobiol.* 2016; 16(1): 1–17.
16. MacDonald M.E., Frayne R. Phase contrast MR imaging measurements of blood flow in healthy human cerebral vessel segments. *Physiol. Measur.* 2015; 36(7): 1517.
17. Su Y, Arbelaez AM, Benzinger TLS, et al. Noninvasive estimation of the arterial input function in positron emission tomography imaging of cerebral blood flow. *J. Cereb. Blood Flow Metab.* 2013; 33(1): 115–121.
18. Lassila T, Di Marco LY, Mitolo M, et al. Screening for cognitive impairment by model assisted cerebral blood flow estimation. *IEEE Trans. Biomed. Eng.* 2018; 65(7): 1654–1661.
19. De Simone G, Devereux RB, Daniels SR, et al. Stroke volume and cardiac output in normotensive children and adults. *Circulation* 1997; 95(7): 1837–1843.

20. Mader G, Olufsen M, Mahdi A. Modeling cerebral blood flow velocity during orthostatic stress. *Ann. Biomed. Eng.* 2015; 43(8): 1748–1758.
21. Krejza J, Szydlak P, Liebeskind DS, et al. Age and sex variability and normal reference values for the VMCA/VICA index. *Am. J. Neuroradiol.* 2005; 26(4): 730–735.
22. Boccadifuoco A, Mariotti A, Celi S, Martini N, Salvetti MV. Impact of uncertainties in outflow boundary conditions on the predictions of hemodynamic simulations of ascending thoracic aortic aneurysms. *Comput. Fluids* 2018; 165: 96–115.
23. Meng H, Tutino VM, Xiang J, Siddiqui A. High WSS or low WSS? Complex interactions of hemodynamics with intracranial aneurysm initiation, growth, and rupture: toward a unifying hypothesis. *Am. J. Neuroradiol.* 2014; 35(7): 1254–1262.
24. Vlak MHM, Rinkel GJE, Greebe P, Algra A. Risk of rupture of an intracranial aneurysm based on patient characteristics: a case–control study. *Stroke* 2013; 44(5): 1256–1259.
25. Vlak MHM, Rinkel GJE, Greebe P, Bom v. dJG, Algra A. Trigger factors and their attributable risk for rupture of intracranial aneurysms: a case-crossover study. *Stroke* 2011; 42(7): 1878–1882.
26. Villa-Uriol MC, Berti G, Hose DR, et al. @neurIST: complex information processing toolchain for the integrated management of cerebral aneurysms. *Interface Focus* 2011: rsfs20100033.
27. Ogoh S, Fadel PJ, Zhang R, et al. Middle cerebral artery flow velocity and pulse pressure during dynamic exercise in humans. *Am. J. Physiol. Heart. Circ. Physiol.* 2005; 288(4): H1526–H1531.
28. Janiga G, Berg P, Sugiyama S, Kono K, Steinman D. The computational fluid dynamics rupture challenge 2013 – phase I: prediction of rupture status in intracranial aneurysms. *Am. J. Neuroradiol.* 2015; 36(3): 530–536.
29. Ingebrigtsen T, Morgan M, Faulder K, Ingebrigtsen L, Sparr T, Schirmer H. Bifurcation geometry and the presence of cerebral artery aneurysms. *J. Neurosurg.* 2004; 101(1): 108–113.
30. Haddad T, Himes A, Thompson L, Irony T, Nair R, others . Incorporation of stochastic engineering models as prior information in Bayesian medical device trials. *J. Biopharm. Stat.* 2017; 27(6): 1089–1103.
31. Miller KL, Alfaro-Almagro F, Bangerter NK, et al. Multimodal population brain imaging in the UK Biobank prospective epidemiological study. *Nat. Neurosci.* 2016; 19(11): 1523.
32. Fisher J, Hartwich D, Seifert T, et al. Cerebral perfusion, oxygenation and metabolism during exercise in young and elderly individuals. *J. Physiol.* 2013; 591(7): 1859–1870.

